A Dual-Channel Naked-Eye Fluorescent Probe for Discriminative Detection of Sulfur Dioxide and Hydrazine

Sha Li *, Yu Hao , Jun Zheng , Xingao Zhang

Posted Date: 15 October 2024

doi: 10.20944/preprints202410.1168.v1

Keywords: dual-channel; fluorescent probe; Naked-Eye; sulfur dioxide; hydrazine

Article

A Dual-Channel Naked-Eye Fluorescent Probe for Discriminative Detection of Sulfur Dioxide and Hydrazine

Sha Li *, Yu Hao, Jun Zheng and Xingao Zhang

Department of Chemistry, Xinzhou Teachers University, Xinzhou 034000, China
* Correspondence: lisaa0612@163.com

Abstract: Hydrazine (N_2H_4) plays an important role in industrial production, but it is highly toxic, leakage or exposure will pollute the environment and cause serious harm to the human body. Sulfur dioxide (SO_2) is an important gas signaling molecule, but its excessive intake can cause a variety of diseases. However, due to the lack of two-color probes capable of detecting both N_2H_4 and SO_2, the ability to monitor the crosstalk of these substances is limited. Therefore, it is necessary to find a simple and effective method for dual-response detection of N_2H_4 and SO_2 in environmental systems and organisms. Here, we developed a two-response fluorescence probe **PI-CO-NH** based on FRET regulation to detect N_2H_4 and SO_2. The experimental results show that the probe has high selectivity and sensitivity, excellent stability, low cytotoxicity and high cell permeability, can visualize N_2H_4 and SO_2 in living cells, and has good mitochondrial targeting ability. It is worth noting that the ability of the probe to detect N_2H_4 in different soil samples and test strips was successfully verified. **PI-CO-NH** provides a platform for the analysis and visualization of two biologically active and environmentally important species, which has great potential in the analysis and monitoring of environmental pollutants.

Keywords: dual-channel; fluorescent probe; Naked-Eye; sulfur dioxide; hydrazine

1. Introduction

SO_2 is a colorless, pungent gas. SO_2 can quickly generate sulfites after being inhaled into the human body. SO_2 can be produced endogenous in the body and has a unique physiological regulation effect in the cardiovascular system [1–3]. However, excessive SO_2 can produce toxic effects on humans and animals, leading to adverse reactions and diseases [4–7]. Excessive intake of SO_2 may lead to asthma, allergic reactions, cardiovascular disease, and neurological disorders [8–10]. In addition, SO_2 is also an environmental pollutant, which easily reacts with water in the atmosphere to produce acid rain, causing harm to the ecological environment. Because of its importance to human health and the environment, it has received great attention. As an important chemical raw material, hydrazine (N_2H_4) inevitably poses a potential threat to the environment and human health in the process of production and use. At the same time, N_2H_4 is also a highly toxic substance, and the human body does not produce endogenous N_2H_4, but N_2H_4 can enter the human body through the skin, respiratory tract or digestive tract, causing damage to the liver, lung, kidney and central nervous system of the human body, and in severe cases, lead to organ failure and threaten life [11–15]. According to the official regulations of the United States Environmental Protection Agency (USEPA), the threshold for N_2H_4 residues in drinking water should be strictly controlled at a level of less than 10 ppb [16–20]. Therefore, it is of great significance to develop a dual-function, efficient and sensitive method for the detection of N_2H_4 and SO_2 in environmental and biological samples.

As a new molecular recognition and detection technology, fluorescence probe technology has the advantages of high sensitivity, good selectivity and fast response speed, and has been widely used in biomedicine, environmental monitoring and other fields [21–29]. Due to its deep tissue penetration ability, low background interference and high light stability, near-infrared (NIR)

 doi:10.20944/preprints202410.1168.v1

fluorescent probes have shown great application potential in biological imaging, medical diagnosis and environmental monitoring and other fields [30]. So far, a large number of fluorescent probes have been reported for the detection of SO_2 and N_2H_4 in biological and environmental systems, but most of them can only detect one analyte [31–36], and few fluorescent probes can detect both SO_2 and N_2H_4. The multifunctional fluorescent probe breaks through the limitation that only a single fluorescent analyte can detect a single analyte, and has more applications and detection efficiency. Simultaneous differential detection of SO_2 and N_2H_4 can avoid optical crosstalk, metabolism, and different localization of multiple probes in vivo, while maintaining cost-effectiveness, less time consumption, and non-invasive imaging [37–40].

Based on this, we designed and developed a novel fluorescence probe based on piperazine-replaced benzopyranium salt combined with coumarin carboxylic acid, and then mihalic acid and 4-(diethylamino)-2-hydroxybenzaldehyde as raw materials, which also has a two-site FRET regulation strategy. The probe has excellent luminescence performance and low toxicity, including benzopyranium salt containing oxygen ions with excellent mitochondrial localization function, adding SO_2 reaction double bond break, red light quenching; Acetyl is a response site for N_2H_4 (Scheme 2). These response groups can detect N_2H_4 and SO_2 separately or simultaneously by means of emission fluctuations, thereby minimizing overlap in the probe spectral range. In addition, it was confirmed in cell experiments that the probe **PI-CO-NH** can detect N_2H_4 and SO_2 in living cells. **PI-CO-NH** has also been successfully applied to soil and test strips, and we hope that the current work can provide good prospects for monitoring N_2H_4 and SO_2 in environmental and biological systems.

2. Experimental Section

2.1. Materials and Instruments

Drugs and solvents used are analytical pure are purchased from suppliers in the experiments and do not need further purification. All chemicals from Aladdin were used without further purification. Fluorescence spectra were carried out a HITACHI F-7000 spectrophotometer. UV-visible spectra were recorded with a HITACHI U-3900 spectrophotometer. NMR spectra were recorded on a JBruker AVANCE-600MHz spectrometer and chemical shifts were referenced relative to tetramethylsilane. Mass data (ESI) were obtained by an AB Triple TOF 5600plus System (AB SCIEX, Framingham, USA). The final bioimaging application were measured by the Zeiss LSM880 Airyscan confocal laser scanning microscope.

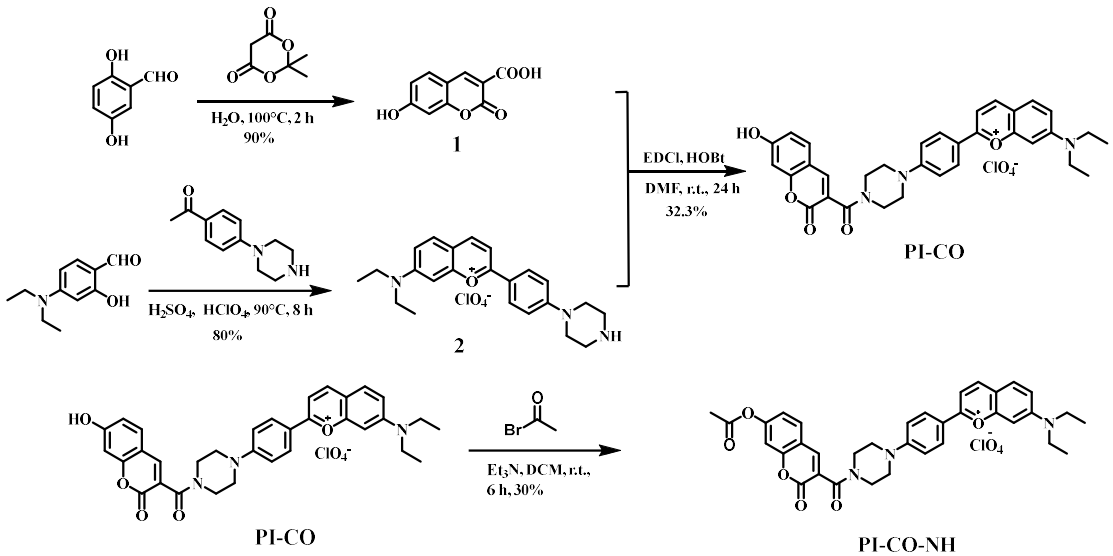

Scheme 1. The synthesis of the probe **PI-CO-NH**.

 doi:10.20944/preprints202410.1168.v1

2.2. The Preparation and Characterization of PI-CO-NH

Compound 1 and **compound 2** were synthesized by a method reported in the literature [41,42].

To a solution of **compound 1** (0.103 g, 0.5 mmol) were added 1-ethyl-3-(3-dimethylaminopropyl) carbodiimide hydrochloride (EDCl, 0.380 g, 2 mmol) and 1-hydroxybenzotriazole (HOBt, 0.270 g, 2 mmol), and the resulting mixture was stirred in dried DMF (15 mL) at 0 ◦C under N_2 for 30 min. Then, **compound 2** (0.230 g, 0.5 mmol) and triethyl-amine (200 μL) were sequentially added. The resulting mixture was stirred at room temperature for 24 h, and then poured into water and washed with cold water to afford an black solid. This powder was purified by column chromatography on silica (methanol/dichloromethane = 1:10 v/v) to afford probe **PI-CO** (0.105 g, 32.3%)

PI-CO (0.088 g, 0.16 mmol), acetyl bromide (0.04 g, 0.32 mmol) and trimethylamine (45 μL, 0.32 mmol) were dissolved in CH_2Cl_2 (5 mL) and the mixture was stirred 6 h at room temperature. The solution was concentrated and was purified by column chromatography to get a dark purple solid **PI-CO-NH** (0.028 g, yield: 30%). 1H NMR (600 MHz, DMSO-d6) δ 8.73 (d, J = 8.1 Hz, 1H), 8.65 (d, J = 8.4 Hz, 1H), 8.29 (d, J = 8.7 Hz, 2H), 8.00 (d, J = 7.9 Hz, 2H), 7.92 (d, J = 9.2 Hz, 1H), 7.66 (s, 1H), 7.50 (d, J = 8.4 Hz, 1H), 7.37 (d, J = 9.0 Hz, 1H), 7.31 (s, 1H), 7.21 (d, J = 8.6 Hz, 2H), 7.07 (d, J = 8.3 Hz, 1H), 3.78 (d, J = 40.8 Hz, 4H), 3.72 – 3.60 (m, 8H), 2.25 (d, J = 8.1 Hz, 3H), 1.25 (s, 7H) (Figure S1 and S2). HS-MS m/z: $[M]^+$ calcd for 592.24; Found 592.30 (Figure S3).

2.3. Solution Preparation and Optical Measurement

The **PI-CO-NH** was dissolved in DMSO to make a 2 mM stock solution. Stock solutions of N_2H_4 and SO_2 were prepared by direct dissolution in deionized water. Various ions (NO_3^-; I^-; SO_3^{2-}; $S_2O_3^{2-}$; Br^-; Cl^-; F^-; NO_2^-; CH_3COO^-; OH^-; $\cdot O_2$; $ONOO^-$; Cys; Glycine; GSH; H_2O_2; Hcy; L-Cystine; L-Glutamate; L-Lysine ; L-Proline; SO_4^{2-}; SNP; K^+; Na^+; Mg^{2+}; Ca^{2+}) were prepared in deionized water. All tests were completed in HEPES buffer (pH 7.4, containing 30% CH_3OH, v/v). Hela cells were used for cell imaging studies.

3. Results and Discussion

3.1. Responding Mechanism of PI-CO-NH

The identification mechanism of **PI-CO-NH** is speculated as follows (Scheme 2). The acetyl group linked by the ether bond is the recognition site for N_2H_4, and the reaction with hydrazine first attacks the carbonyl group of the acetyl group, and then causes the ester group to break down, causing coumarin to glow blue. After adding SO_2, the double bond on benzopyrrole was broken and the red fluorescence was quenched. To further investigate the response mechanism, we validated the corresponding HRMS characterization of **PI-CO-NH** with N_2H_4 and SO_2. These results provide support for our proposed probe (**PI-CO-NH**) to distinguish between N_2H_4 and SO_2.

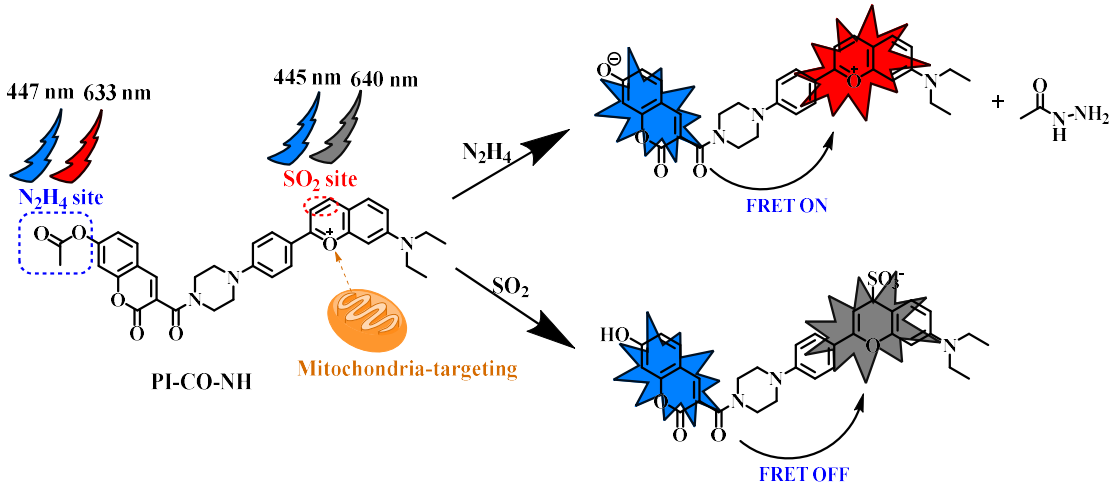

Scheme 2. The synthesis of the probe **PI-CO-NH**.

 doi:10.20944/preprints202410.1168.v1

3.2. UV–Visible Absorption Spectra of PI-CO-NH

First, we studied the UV-visible spectra of **PI-CO-NH** for N_2H_4 in HEPES buffer (pH 7.4, containing 30 % CH_3OH, v/v). As shown in Figure 1A, **PI-CO-NH** has a peak at 447 nm and 633 nm, respectively. After adding N_2H_4, the absorption peak at 447 nm is gradually enhanced, and the absorption peak at 633 nm is gradually weakened. The appearance of new peaks indicates that the ester group in the probe structure is destroyed and combines with N_2H_4 to form a new substance.

Then the UV–visible response of **PI-CO-NH** for N_2H_4 in HEPES buffer (pH 7.4, containing 30 % CH_3OH, v/v) was tested. It can be seen from Figure 1B that **PI-CO-NH** has strong absorption peaks at 425 nm and 580 nm. With the addition of SO_2, the absorption peak at 425 nm increased significantly and the absorption peak at 580 nm decreased significantly. It was concluded that the double bond of **PI-CO-NH** reacted with SO_2 was broken, and the solution changed from blue purple to colorless. This phenomenon shows that **PI-CO-NH** can be used as a colorimetric probe and can be identified with the "naked eye".

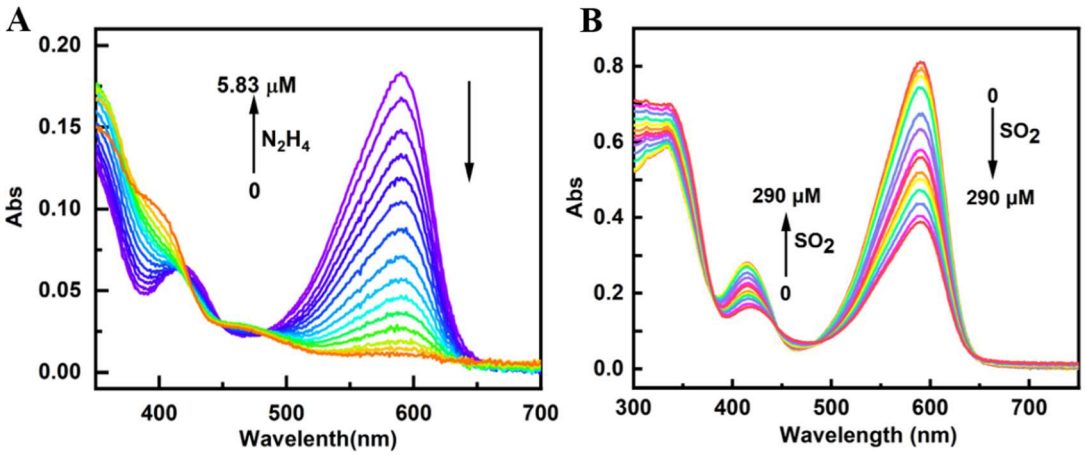

Figure 1. UV-Vis absorption spectra of **PI-CO-NH** towards N_2H_4 and SO_2 in the HEPES buffer (pH 7.4, containing 30% CH_3OH, v/v).

3.3. Fluorescence Spectra of PI-CO-NH

The fluorescence intensity of **PI-CO-NH** for N_2H_4 and SO_2 was detected in HEPES buffer (pH 7.4, containing 30% CH_3OH, v/v). As shown in Figure 2AB, when N_2H_4 was added, the ether bond breaks, releasing a red fluorescence of 633 nm. At the same time, the fluorescence intensity at 447 nm gradually increased with the increase of concentration. The significant increase in fluorescence intensity is due to the blocking of the PET process from PI-CO to acetyl bromide. In order to test the response of **PI-CO-NH** to SO_2 (Figure 2CD), an emission peak appeared at 640 nm under 580 nm excitation, and the fluorescence intensity gradually decreased with the addition of SO_2. The results show that **PI-CO-NH** can achieve rapid detection of SO_2.

 doi:10.20944/preprints202410.1168.v1

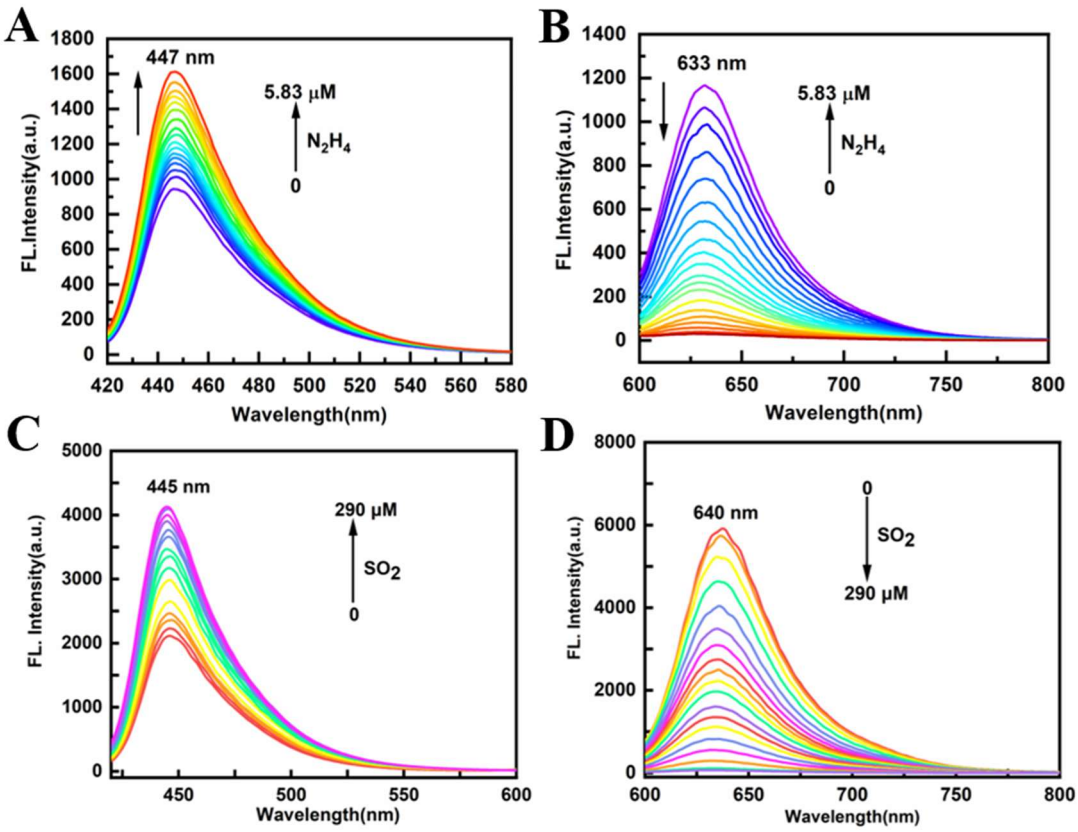

Figure 2. Fluorescence spectra of **PI-CO-NH** (10 mM) with (A-B) N_2H_4 (0-5.83 μM) (C-D) SO_2 (0-290 μM) in the HEPES buffer (pH 7.4, containing 30% CH_3OH, v/v). A, C: λ_{ex}=420 nm, Ex/Em slit: 5/5 nm; B, D: λ_{ex}=580 nm, Ex/Em slit: 5/5 nm.

In order to determine the linear response range of **PI-CO-NH** to N_2H_4 and SO_2, we obtained the corresponding curve by using the concentration of N_2H_4 and SO_2 as the transverse coordinates and the fluorescence intensity as the vertical coordinates (Figure 3). The linear equation of N_2H_4 was y=22.14x+837.5, R^2=0.996 (λ_{ex}=420 nm); y=2.89x+1092, R^2=0.997 (λ_{ex}=580 nm). Further, the linear equation of SO_2 was y=27.06x+3142.84, R^2=0.998 (λ_{ex}=420 nm). Besides, The linear equation of SO_2 was y=-118.477x+5837.79, R^2 = 0.987 (λ_{ex}=580 nm).

 doi:10.20944/preprints202410.1168.v1

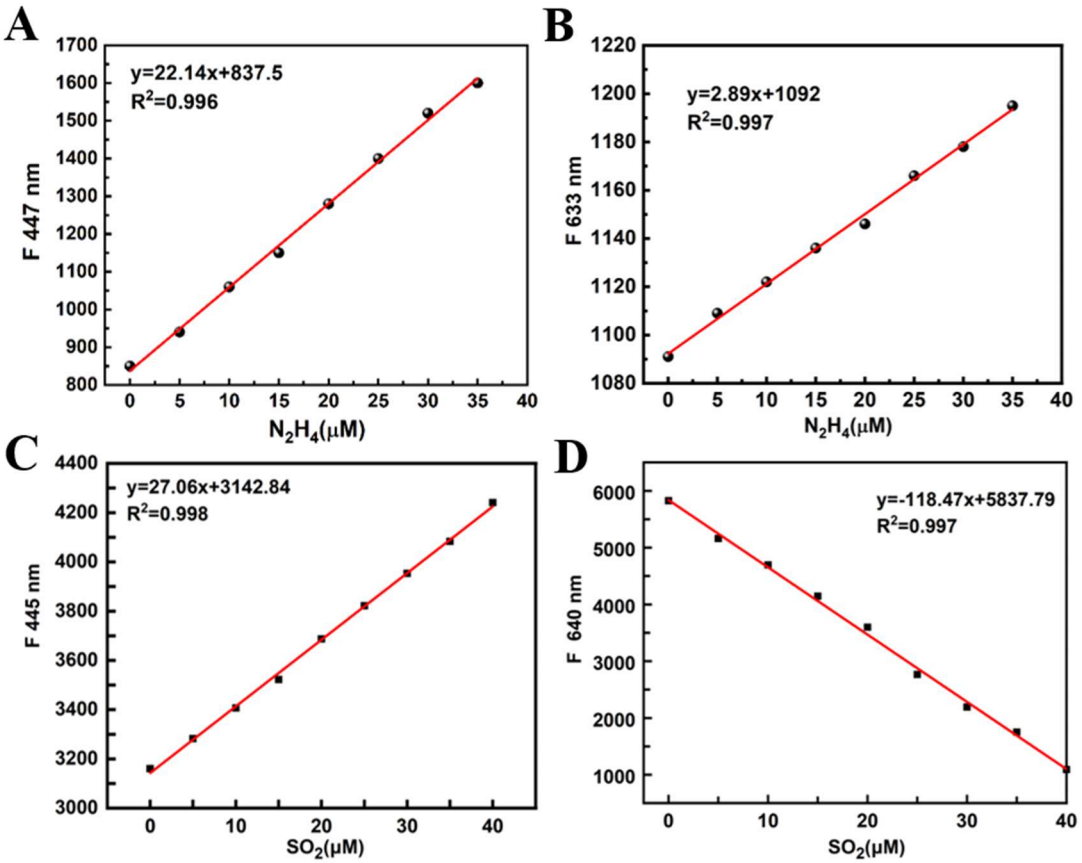

Figure 3. Plot of the fluorescence intensity of **PI-CO-NH** as a function of the N_2H_4 and SO_2 concentration.

3.4. pH Test of PI-CO-NH

To investigate the effects of pH for the fluorescent response of **PI-CO-NH**, the fluorescence intensity of **PI-CO-NH** was measured from pH 2-10 (Figure S2). In the absence of N_2H_4 and SO_2, the fluorescence intensity of **PI-CO-NH** did not apparent changed in the range of pH 2-10. When adding N_2H_4 (SO_2), the emission of **PI-CO-NH** at 447 (640) nm increased significantly with the change of pH, and reached the maximum at neutral condition. These results indicate that **PI-CO-NH** has good sensing performance under physiological conditions.

 doi:10.20944/preprints202410.1168.v1

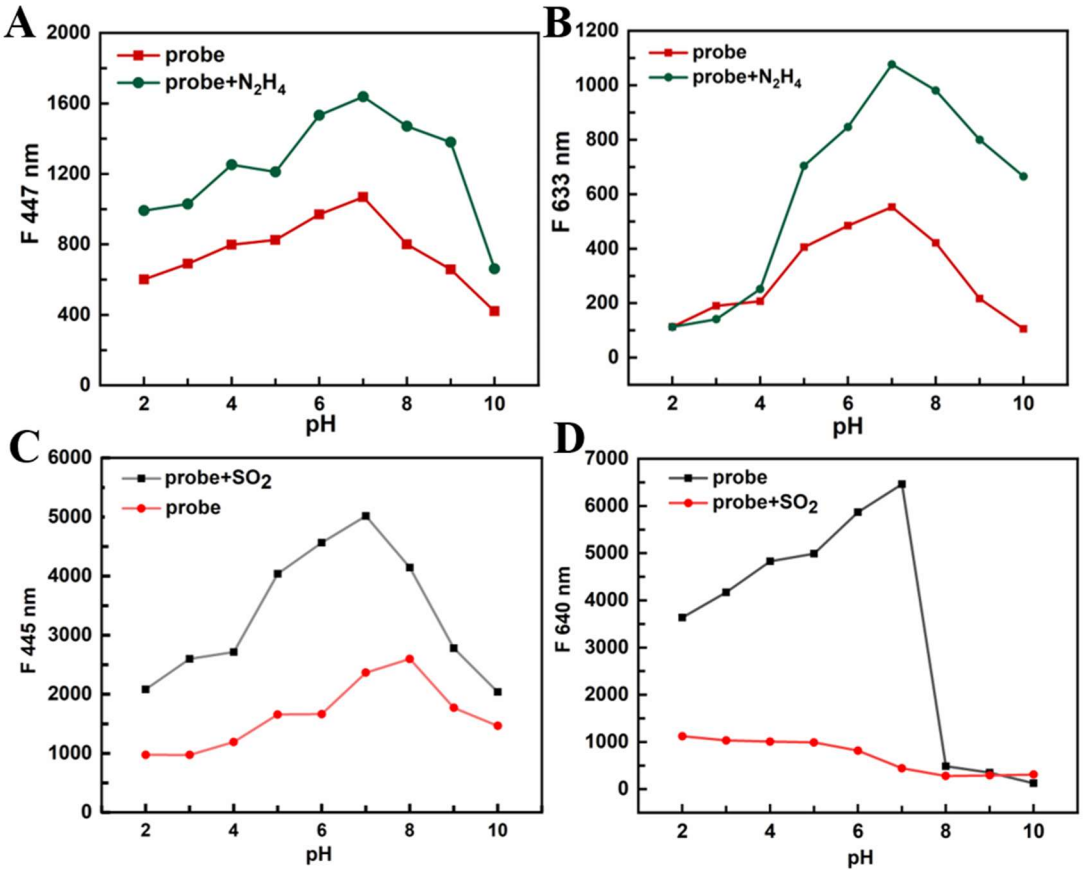

Figure 4. Different pH values fluorescent changes of **PI-CO-NH** in the absence and present of N_2H_4 and SO_2.

3.5. Selective Testing of PI-CO-NH

We evaluated the selectivity of **PI-CO-NH** to N_2H_4 and SO_2 over other amino acids, including NO_3^-; I^-; SO_3^{2-}; $S_2O_3^{2-}$; Br^-; Cl^-; F^-; NO_2^-; CH_3COO^-; OH^-; $\cdot O_2$; $ONOO^-$; Cys; Glycine; GSH; H_2O_2; Hcy; L-Cystine; L-Glutamate; L-Lysine ; L-Proline; SO_4^{2-}; SNP; K^+; Na^+; Mg^{2+}; Ca^{2+}. From Figure 5, only N_2H_4 and SO_2 could cause obvious changes of fluorescence intensity of **PI-CO-NH**, and other amino acids caused negligible fluorescence responses. This showed **PI-CO-NH** had high selectivity to N_2H_4 and SO_2 over other amino acids.

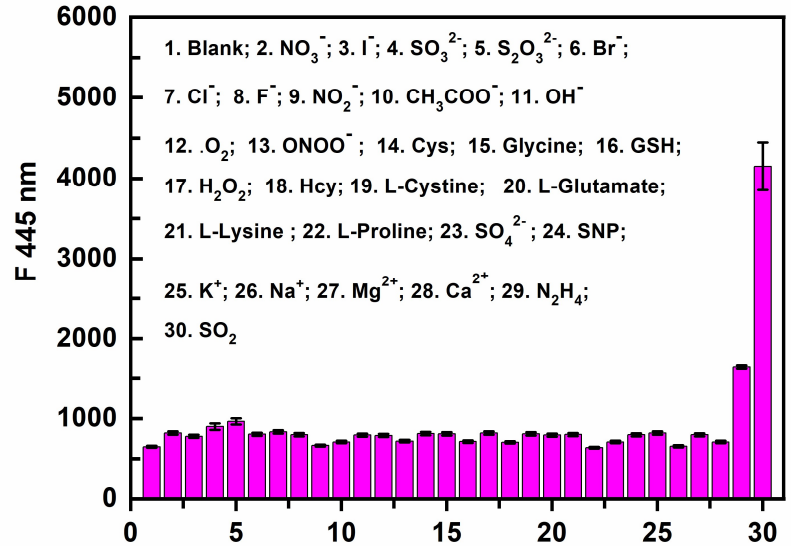

 doi:10.20944/preprints202410.1168.v1

Figure 5. The fluorescence intensity of **PI-CO-NH** with N_2H_4, SO_2 and other amino acids (10 equiv, NO_3^-; I^-; SO_3^{2-}; $S_2O_3^{2-}$; Br^-; Cl^-; F^-; NO_2^-; CH_3COO^-; OH^-; $\cdot O_2$; $ONOO^-$; Cys; Glycine; GSH; H_2O_2; Hcy; L-Cystine; L-Glutamate; L-Lysine ; L-Proline; SO_4^{2-}; SNP; K^+; Na^+; Mg^{2+}; Ca^{2+}) in the HEPES buffer (pH 7.4, containing 30% CH_3OH, v/v) at 445 nm.

3.6. Time Response of PI-CO-NH

The time response of **PI-CO-NH** to N_2H_4 and SO_2 was measured in HEPES buffer (pH 7.4, containing 30% CH_3OH, v/v). After adding N_2H_4, the fluorescence intensity of **PI-CO-NH** significantly increased at 447 nm (Figure 6A). Besides, when added SO_2, the fluorescence intensity drops rapidly. **PI-CO-NH** has good stability.

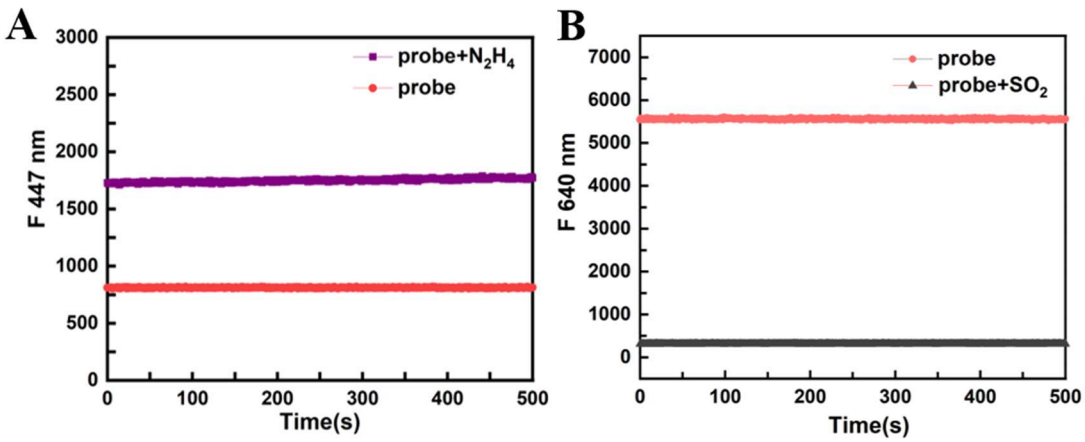

Figure 6. Time response of probe **PI-CO-NH** with N_2H_4 and SO_2.

3.7. Determination of N_2H_4 in Soil Samples and Strips

Based on the fact that the widespread use of N_2H_4 can lead to serious water and soil contamination, we investigated the ability of **PI-CO-NH** to detect N_2H_4 in various soils (sand, clay and field soil) and in test strips. In the soil sample(Figure 7A-B), the probe was first mixed with the soil, and then the fluorescence color under the ultraviolet lamp was observed. Then N_2H_4 was added to the soil mixed with the probe, and the fluorescence color under the ultraviolet lamp was observed again. In the experiment of the test strip (Figure 7C-D), we also did a similar test, dissolve the probe in the water source (Yunzhonghe River), observe the color of the trace left by the liquid on the filter paper under the ultraviolet lamp, and then add N_2H_4 to the liquid mixed with the probe, and observe the color of the trace left by the liquid on the filter paper under the ultraviolet lamp again. The figure shows the different fluorescence patterns of **PI-CO-NH** (red) and **PI-CO-NH** + N_2H_4 (blue) under ultraviolet light. It can be clearly seen from the figure that when **PI-CO-NH** combines with N_2H_4, its fluorescence color changes significantly, rapidly changing from red to blue. This noticeable color change provides a convenient and intuitive way to detect the presence of N_2H_4 in soil and water. This result proves that **PI-CO-NH** can be used for rapid and sensitive detection of N_2H_4 in environmental samples.

 doi:10.20944/preprints202410.1168.v1

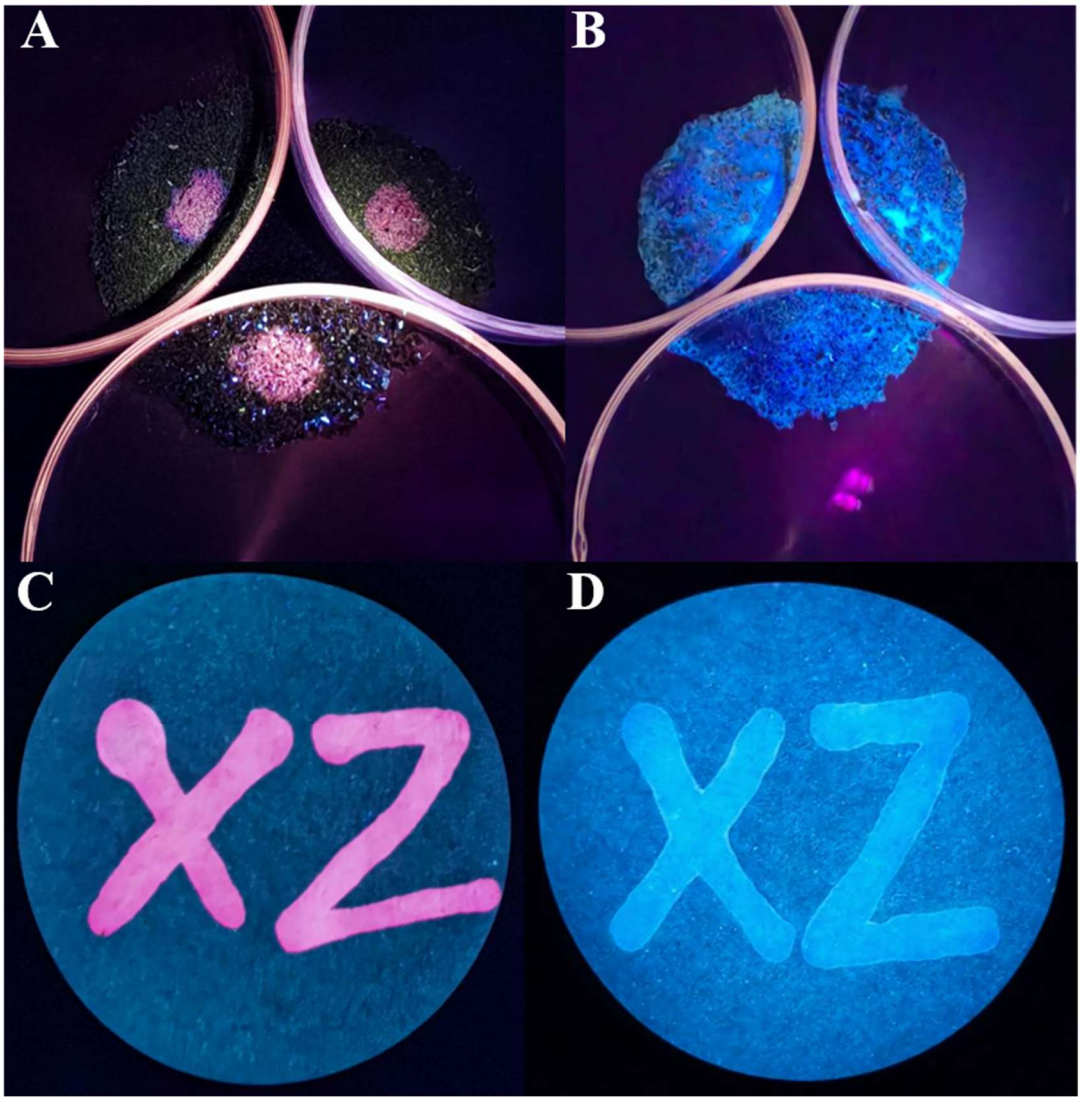

Figure 7. Fluorescence detection of **PI-CO-NH** reaction with N_2H_4 on different soil and test strips.

3.8. Cell Imaging of PI-CO-NH

Based on the excellent response performance of **PI-CO-NH** to N_2H_4 and SO_2 in vitro, we used HeLa cells as model cells to detect the response of **PI-CO-NH** to N_2H_4 and SO_2 in living cells. As shown in Figure 8, when HeLa cells were incubated with only 10 μM **PI-CO-NH** at 37°C for 15 min, weak blue fluorescence was observed. Cells treated with N_2H_4 and incubated with probes showed significantly enhanced fluorescence signals in blue and red channels (Figure 8a2-b2). Cells treated with SO_2 and incubated with the probe showed a significantly reduced fluorescence signal in the red channel (Figure 8a3-8c3). The results showed that **PI-CO-NH** had good cell membrane permeability and could be used for the detection of N_2H_4 and SO_2 at cell level.

To further illustrate the recognition ability of **PI-CO-NH** to N_2H_4, we measured the fluorescence changes of hydrazine at different concentrations (0 μM, 2 μM, 5 μM) during cell incubation. As shown in Figure 9, with the increase of N_2H_4 concentration, the fluorescence of the blue channel is gradually enhanced. Therefore, **PI-CO-NH** can detect different concentrations of N_2H_4 at the cellular level.

 doi:10.20944/preprints202410.1168.v1

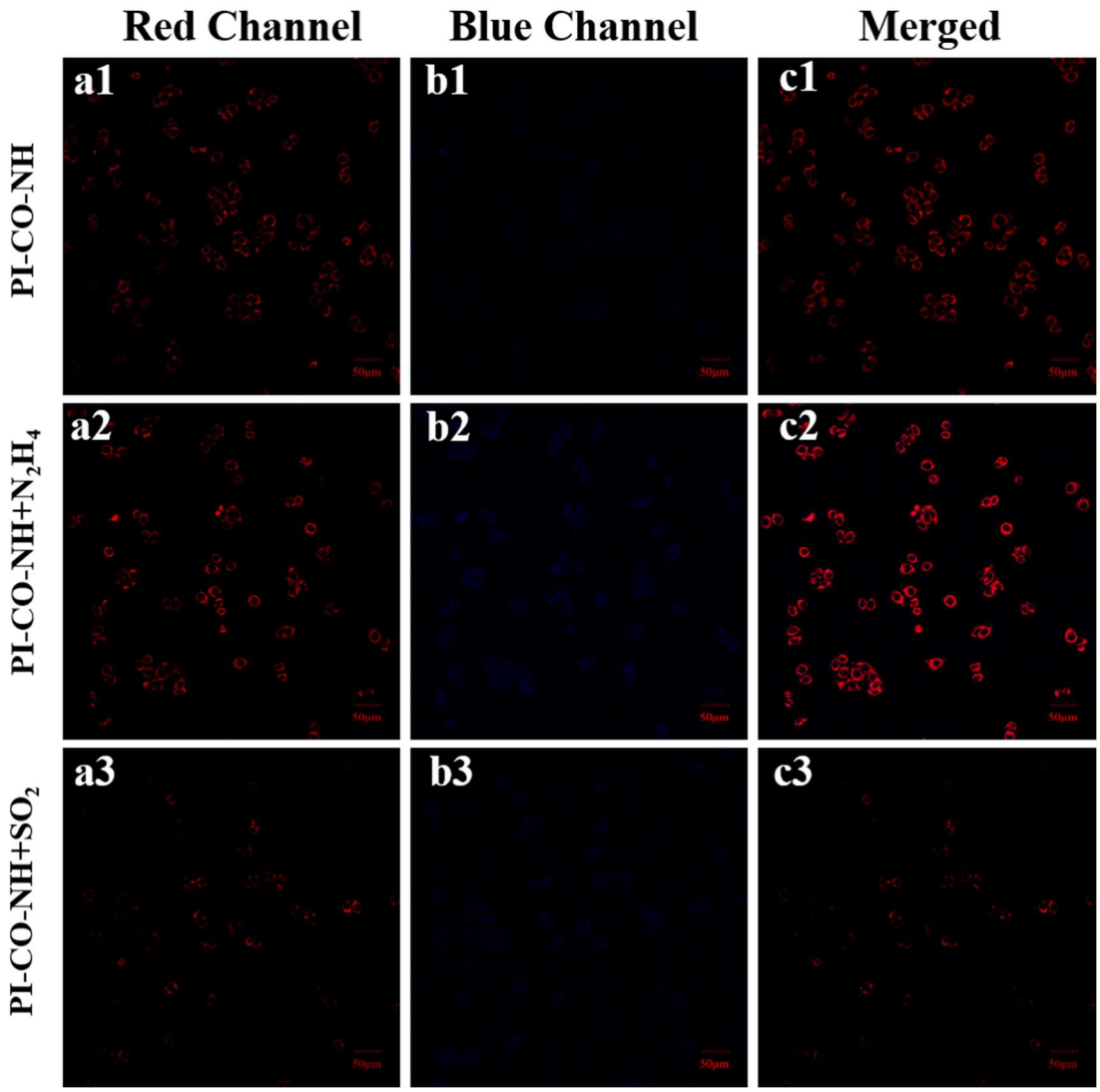

Figure 8. Imaging of hydrazine in HeLa cells. (a1-c1) HeLa cells incubated with **PI-CO-NH**; (a2-c2) HeLa cells incubated with **PI-CO-NH** and further incubated with N_2H_4. (a3-c3) HeLa cells incubated with **PI-CO-NH** and further incubated with SO_2. Blue channel: λ_{ex} = 405 nm, λ_{em} = 490–550 nm; red channel: λ_{ex} = 561 nm, λ_{em} = 610–670 nm.

 doi:10.20944/preprints202410.1168.v1

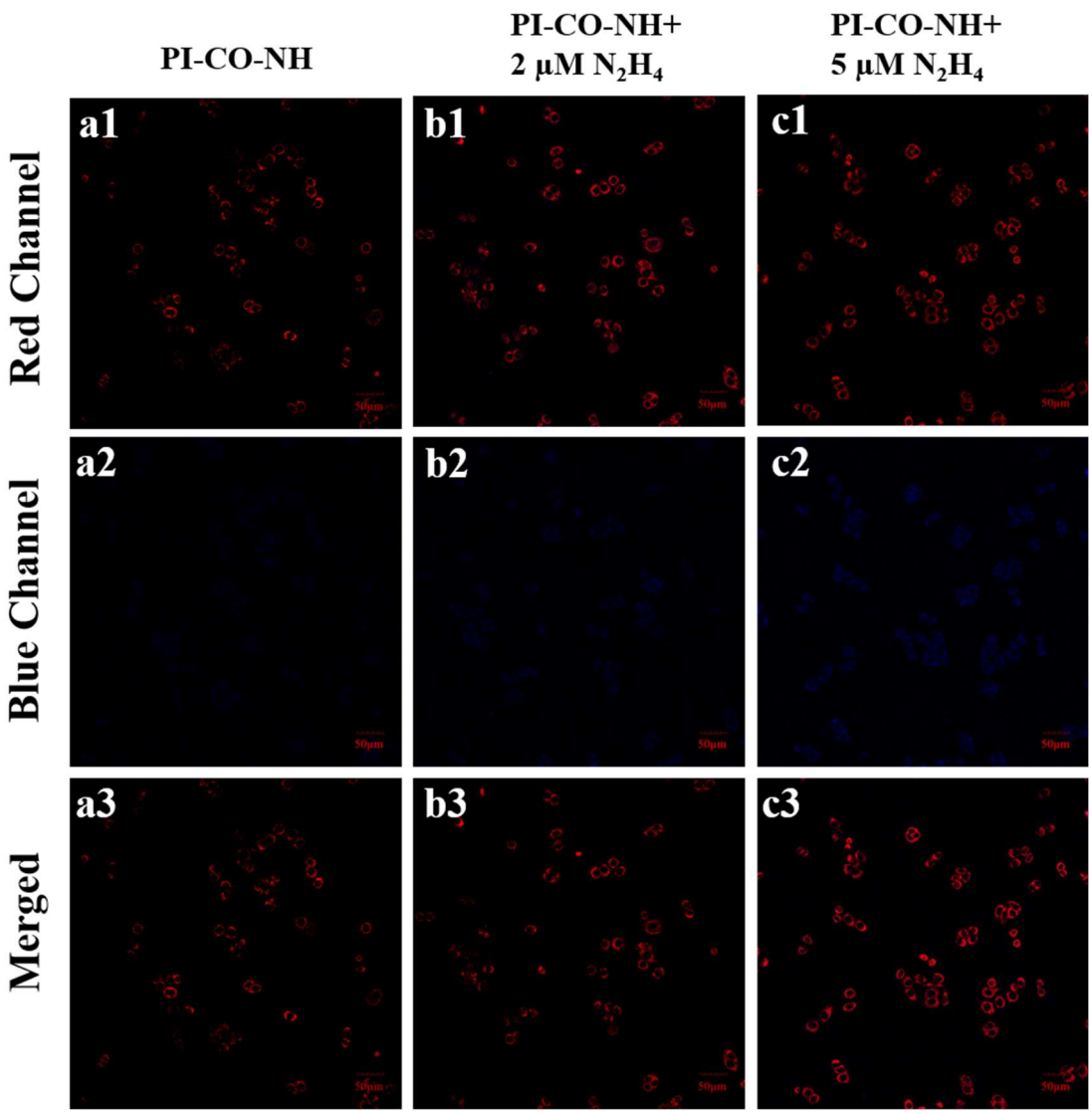

Figure 9. Imaging of N_2H_4 in HeLa cells. (a1-c1) HeLa cells incubated with **PI-CO-NH** (10 μM); (a2-c4) HeLa cells incubated with **PI-CO-NH** and further incubated with N_2H_4 (2 μM, 5 μM). Blue channel: λex = 405 nm, λem = 490–550 nm; red channel: λ_{ex} = 561 nm, λ_{em} = 610–670 nm.

Given that N_2H_4 is toxic to mitochondria, we further explored its mitochondria-targeting ability to determine whether **PI-CO-NH** has the potential to monitor mitochondrial toxicity of N_2H_4 (Figure 10). HeLa cells pretreated with hydrazine were stained with commercially available mitochondrial green targeting reagent and **PI-CO-NH**, respectively. The green fluorescence signal of Mito-tracker Green in HeLa cells basically coincided with the red fluorescence signal of **PI-CO-NH**, and Pearson's coefficient reached 0.87. The above results prove that **PI-CO-NH** has good mitochondrial targeting property and can realize the imaging of both internal and external mitochondrial source hydrazine.

 doi:10.20944/preprints202410.1168.v1

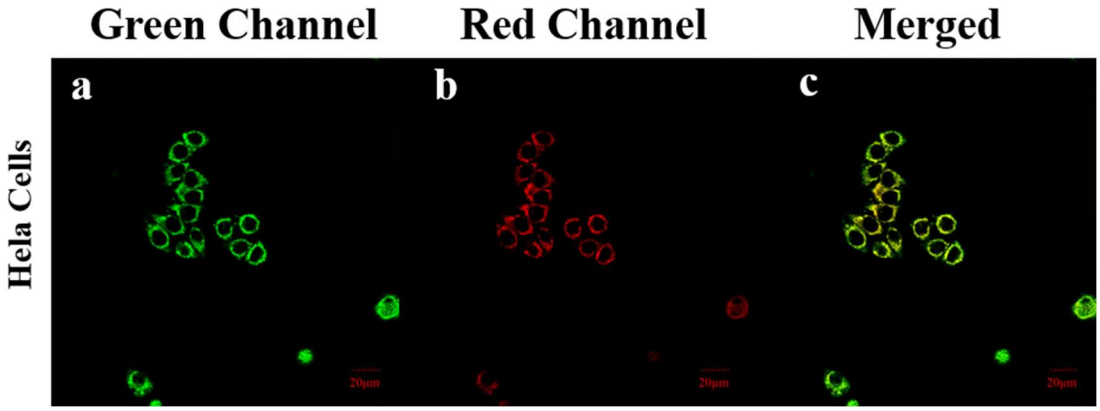

Figure 10. The colocalization fluorescence imaging of HeLa cells co-treated with (a) **PI-CO-NH** (10 μM) and (b) Mito-Tracker Green (500 μM). (c) The merge of the red and green channels. Scale bar: 20 μM. Blue channel: λ_{ex} = 488 nm, λ_{em} = 486-546 nm; Red channel: λ_{ex} = 561 nm, λ_{em} = 700-760 nm.

4. Conclusion

In summary, we have synthesized a novel dual-emission NIR fluorescent probe **PI-CO-NH** based on piperazine-substituted benzopyranone salts and coumarin carboxylic acids, which is a dual-function probe capable of detecting SO_2 or N_2H_4. When detecting SO_2 or N_2H_4, the probe exhibits rapid fluorescence changes with two different emission channels (447 nm and 633 nm) and shows resistance to interference through its independent fluorescence channel and FRET sensing mechanism. The experimental results show that the probe has high selectivity and sensitivity, excellent stability, low cytotoxicity and high cell permeability, can visualize N2H4 and SO2 in living cells, and has good mitochondrial targeting ability. More importantly, the ability of **PI-CO-NH** to detect N_2H_4 in different soil samples and test strips was successfully verified. These experiments not only validate the applicability of the probe in complex environment, but also provide a strong basis for the future application of **PI-CO-NH** in environmental pollution detection.

Acknowledgements: This work was supported by Science and technology innovation project of higher education in Shanxi Province (2023L295) and the Natural Science Foundation of Shanxi Province (202303021222234) and the National Natural Science Foundation of China (No. 22277104).

References

1. M. Wang, L. Cao, Z. Liu, et al., Sulfur dioxide-resistant platinum-based intermetallic nanocatalysts encaged by porous nitrogen-doped carbon for oxygen reduction reaction, Chemical Engineering Journal 492 (2024) 152-162
2. M. Tizfahm, M. Tahmasebpoor, R.H. Behtash, et al., Coupled kinetic and hydrodynamic model for a carbonator reactor of calcium looping process: Sulfur dioxide effect, Process Safety and Environmental Protection 185 (2024) 1205-1218.
3. J.L. Hart, Role of sulfur-containing gaseous substances in the cardiovascular system, Frontiers in Bioscience Elite 3 (2011) 736-749.
4. J. Du, Y. Huang, K. Li, et al., Retina-derived endogenous sulfur dioxide might be a novel anti-apoptotic factor, Biochemical and Biophysical Research Communications 496 (2018) 955-960.
5. Y. Huang, Z. Shen, Q. Chen, et al., Endogenous sulfur dioxide alleviates collagen remodeling via inhibiting TGF-β/Smad pathway in vascular smooth muscle cells, Scientific Reports 6 (2016) 19503.
6. S. Chen, Y. Huang, Z. Liu, et al., Sulphur dioxide suppresses inflammatory response by sulphenylating NF-κB p65 at Cys38 in a rat model of acute lung injury, Clinical Science 131(21) (2017) 2655-2670.
7. Y.-H. Qin, X.-Y. Jiang, Y.-F. Que, J.-Y. Gu, T. Wu, A. Aihemaiti, K.-X. Shi, W.-Y. Kang, B.-Y. Hu, J.-S. Lan, et al., A Ratiometric and Colorimetric Hemicyanine Fluorescent Probe for Detection of SO_2 Derivatives and Its Applications in Bioimaging, Molecules 24 (2019) 4011.
8. Z. Meng, H. Zhang, The vasodilator effect and its mechanism of sulfur dioxide-derivatives on isolated aortic rings of rats, Inhalation Toxicology 19 (2007) 979-986.

9. Q. Chen, L. Zhang, S. Chen, et al., Downregulated endogenous sulfur dioxide/aspartate aminotransferase pathway is involved in angiotensin II-stimulated cardiomyocyte autophagy and myocardial hypertrophy in mice, International Journal of Cardiology 225 (2016) 392-401.
10. S.L. Taylor, N.A. Higley, R.K. Bush, Sulfites in foods: uses, analytical methods, residues, fate, exposure assessment, metabolism, toxicity, and hypersensitivity, Advances in Food Research 30 (1986) 1-76.
11. R.F. McFeeters, Use and removal of sulfite by conversion to sulfate in the preservation of salt-free cucumbers, Journal of Food Protection 61 (1998) 885-890.
12. D.F. Splittstoesser, L.R. Mattic, The storage life of refrigerated grape juice containing various levels of sulfur dioxide, American Journal of Enology and Viticulture 32 (1981) 171-173.
13. X. Sheng, X. Sun, Y. Zhang, C. Zhang, S. Liu, S. Wang, A Ratiometric Fluorescent Probe for N2H4 Having a Large Detection Range Based upon Coumarin with Multiple Applications, Molecules 28 (2023) 7629.
14. J. Wu, J. Pan, Z. Ye, et al., A smart fluorescent probe for discriminative detection of hydrazine and bisulfite from different emission channels, Sensors and Actuators: B. Chemical 2 (2018) 4274-4284.
15. S.G. Hua, Z.G. Qian, C.W. Yun, et al., An ultrasensitive fluorescent probe for hydrazine detection and its application in water samples and living cells, Tetrahedron 18 (2019) 2642-2646.
16. J. Du, X. Li, S. Ruan, et al., Rational design of a novel turn-on fluorescent probe for the detection and bioimaging of hydrazine with barbituric acid as a recognition group, Analyst 2 (2019) 636-642.
17. M. Du, Y. Zhang, Z. Xu, Z. Dong, S. Zhao, H. Du, H. Zhao, Point-of-Care and Dual-Response Detection of Hydrazine/Hypochlorite-Based on a Smart Hydrogel Sensor and Applications in Information Security and Bioimaging, Molecules 28 (2023) 3896-3960.
18. A. Serov, M. Padilla, A.J. Roy, P. Atanassov, T. Sakamoto, K. Asazawa, H. Tanaka, Anode catalysts for direct hydrazine fuel cells: from laboratory test to an electric vehicle, Angew Chem. Int. Ed. Engl. 53 (39) (2014) 10336–10340.
19. N. Nobari, M. Behboudnia, R. Maleki, Palladium-free electroless deposition of pure copper film on glass substrate using hydrazine as reducing agent, Appl. Surf. Sci. 385 (2016) 9–17.
20. L. Yi, G.D. Yao, Z. Heng, B.B. Jin, Rapid catalytic reduction of NaHCO3 into formic acid and methane with hydrazine over Raney Ni catalyst, Catal. Today 298 (2017) 124–129.
21. Z. Chen, X.X. Zhong, W.B. Qu, T. Shi, H. Liu, H.P. He, X.H. Zhang, S.F. Wang, A highly selective HBT-based “turn-on” fluorescent probe for hydrazine detection and its application, Tetrahedron Lett. 58 (26) (2017) 2596–2601.
22. Y.B. Ding, S. Zhao, Q.Q. Wang, X. Yu, W.H. Zhang, Construction of a coumarin based fluorescent sensing platform for palladium and hydrazine detection, Sensor Actuat B Chem. 256 (2018) 1107–1113.
23. S. Mu, H. Gao, C. Li, S. Li, Y. Wang, Y. Zhang, C. Ma, H. Zhang, X. Liu, A dualresponse fluorescent probe for detection and bioimaging of hydrazine and cyanide with different fluorescence signals, Talanta 221 (2021) 121606–121614.
24. M. Zhu, Z. Zhao, Y. Huang, F. Fan, F. Wang, W. Li, X. Wu, R. Hua, Y. Wang, Hydrazine exposure: a near-infrared ICT-based fluorescent probe and its application in bioimaging and sewage analysis, Sci. Total Environ. 759 (2021) 143102–143111.
25. C.S. Patil, D.B. Gunjal, V.M. Naik, N.S. Harale, S.D. Jagadale, A.N. Kadam, P. S. Patil, G.B. Kolekar, A.H. Gore, Waste tea residue as a low cost adsorbent for removal of hydralazine hydrochloride pharmaceutical pollutant from aqueous media: an environmental remediation, J. Clean. Prod. 206 (2019) 407–418.
26. S. Garrod, M.E. Bollard, A.W. Nicholls, S.C. Connor, J. Connelly, J.K. Nicholson, E. Holmes, Integrated metabonomic analysis of the multiorgan effects of hydrazine toxicity in the Rat, Chem. Res. Toxicol. 18 (2) (2005) 115–122.
27. J.K. Niemeier, D.P. Kjell, Hydrazine and aqueous hydrazine solutions: evaluating safety in chemical processes, Org. Process Res. Dev. 17 (12) (2013) 1580–1590.
28. J.H. Ma, J.L. Fan, H.D. Li, Q.C. Yao, J. Xia, J.Y. Wang, X.J. Peng, Probing hydrazine with a near-infrared fluorescent chemodosimeter, Dyes Pigments 138 (2017) 39–46.
29. A.A. Ensafi, B.J. Naderi, Flow-injection spectrophotometric determination of hydrazine, Microchem. J. 56 (3) (1997) 269–275.
30. H. Singh, K. Tiwari, R. Tiwari, S.K. Pramanik, A. Das, Small molecule as fluorescent probes for monitoring intracellular enzymatic transformations, Chem. Rev. 119 (22) (2019) 11718–11760.
31. X.-Y. Zhang, Y.-S. Yang, W. Wang, Q.-C. Jiao, H.-L. Zhu, Fluorescent sensors for the detection of hydrazine in environmental and biological systems: recent advances and future prospects, Coord. Chem. Rev. 417 (2020), 213367.
32. X. Chen, K.-A. Lee, X. Ren, J.-C. Ryu, G. Kim, J.-H. Ryu, W.-J. Lee, J. Yoon, Synthesis of a highly HOCl-selective fluorescent probe and its use for imaging HOCl in cells and organisms, Nat. Protoc. 11 (7) (2016) 1219–1228.
33. X. Shi, F. Huo, J. Chao, C. Yin, A ratiometric fluorescent probe for hydrazine based on novel cyclization mechanism and its application in living cells, Sens. Actuators B Chem. 260 (2018) 609–616.

 doi:10.20944/preprints202410.1168.v1

34. X. Kong, B. Dong, C. Wang, N. Zhang, W. Song, W. Lin, A novel mitochondriatargeted fluorescent probe for imaging hydrazine in living cells, tissues and animals, J. Photochem. Photobiol. A: Chem. 356 (2018) 321–328.
35. S. Yu, S. Wang, H. Yu, Y. Feng, S. Zhang, M. Zhu, H. Yin, X. Meng, A ratiometric two-photon fluorescent probe for hydrazine and its applications, Sens. Actuators B Chem. 220 (2015) 1338–1345.
36. S. Wang, S. Ma, J. Zhang, M. She, P. Liu, S. Zhang, J. Li, A highly sensitive and selective near-infrared fluorescent probe for imaging hydrazine in living tissues and mice, Sens. Actuators B Chem. 261 (2018) 418–424.
37. B. Wang, R. Yang, W. Zhao, Construction of a mitochondria-targeted ratiometric fluorescent probe for monitoring hydrazine in soil samples and culture cells, J. Hazard. Mater. 406 (2021), 124589.
38. Z. Wang, Y. Zhang, Z. Meng, M. Li, C. Zhang, L. Yang, Y. Yang, X. Xu, S. Wang, Development of a ratiometric fluorescent probe with large Stokes shift and emission wavelength shift for real-time tracking of hydrazine and its multiple applications in environmental analysis and biological imaging, J. Hazard. Mater. 422 (2022),126891.
39. M. Oguz, S. Erdemir, S. Malkondu, An effective benzothiazole-indandione D-π-A fluorescent sensor for “ratiometric” detection of hydrazine: its solvatochromism properties and applications in environmental samples and living cells, Anal. Chim. Acta 1227 (2022), 340320.
40. S. Erdemir, M. Oguz, S. Malkondu, Real-time screening of hydrazine by a NIR fluorescent probe with low cytotoxicity in living cells and its multiple applications: optimization using Box-Behnken Design, Sens. Actuators B Chem. 364 (2022), 131893
41. W. J. Cheng, Y. T. Xie, Z. Y. Yang, Y. Q. Sun, M. Z. Zhang, Y. B. Ding, W. H. Zhang, Anal. Chem. 91 (2019) 5817–5823.
42. W. J. Zhang, F. J. Huo, F. Q. Cheng, C. X. Yin, J. Am. Chem. So.c 142 (2020) 6324–6331.